Cell-type–specific inhibition of the dendritic plateau potential in striatal spiny projection neurons

Kai Du[a,b,1], Yu-Wei Wu[c,d,1], Robert Lindroos[a,b], Yu Liu[c,d], Balázs Rózsa[e], Gergely Katona[f], Jun B. Ding[c,d,2,3], and Jeanette Hellgren Kotaleski[a,b,g,2,3]

[a]Stockholm Brain Institute, Karolinska Institute, 171 77 Solna, Sweden; [b]Department of Neuroscience, Karolinska Institute, 171 77 Solna, Sweden; [c]Department of Neurosurgery, Stanford University School of Medicine, Stanford, CA 94305; [d]Department of Neurology and Neurological Sciences, Stanford University School of Medicine, Stanford, CA 94305; [e]Laboratory of 3D Functional Imaging of Neuronal Networks and Dendritic Integration, Institute of Experimental Medicine, Hungarian Academy of Sciences, 1083 Budapest, Hungary; [f]Magyar Tudományos Akadémia–Pázmány Páter Katolikus Egyetem, Információs Technológia Kar–Nemzeti Agykutatás Program (MTA-PPKE ITK-NAP) Two-Photon Measurement Technology Research Group, Pázmány Péter University, 1088 Budapest, Hungary; and [g]Science for Life Laboratory, School of Computer Science and Communication, KTH Royal Institute of Technology, 114 28 Stockholm, Sweden

Edited by Thomas C. Südhof, Stanford University School of Medicine, Stanford, CA, and approved July 18, 2017 (received for review March 23, 2017)

Striatal spiny projection neurons (SPNs) receive convergent excitatory synaptic inputs from the cortex and thalamus. Activation of spatially clustered and temporally synchronized excitatory inputs at the distal dendrites could trigger plateau potentials in SPNs. Such supralinear synaptic integration is crucial for dendritic computation. However, how plateau potentials interact with subsequent excitatory and inhibitory synaptic inputs remains unknown. By combining computational simulation, two-photon imaging, optogenetics, and dual-color uncaging of glutamate and GABA, we demonstrate that plateau potentials can broaden the spatiotemporal window for integrating excitatory inputs and promote spiking. The temporal window of spiking can be delicately controlled by GABAergic inhibition in a cell-type–specific manner. This subtle inhibitory control of plateau potential depends on the location and kinetics of the GABAergic inputs and is achieved by the balance between relief and reestablishment of NMDA receptor Mg^{2+} block. These findings represent a mechanism for controlling spatiotemporal synaptic integration in SPNs.

dendritic computation | inhibition | plateau potential | synaptic integration | striatum

One of the principal functions of neurons is to integrate excitatory and inhibitory synaptic inputs and transform subthreshold membrane potential fluctuations into suprathreshold spiking activities. Both theoretical and experimental works have proposed that a single neuron can process inputs as a multilayer computational device in which individual dendritic branches function as a computational unit and can generate dendritic spikes or plateau potentials (1–4). In vivo studies have demonstrated that dendritic plateau potentials evoked by coincident inputs can amplify excitatory signals and enhance the capacity of learning and information storage at a specific branch (5–7). However, a majority of the understanding of dendritic computation is based on studies focusing on pyramidal cells of hippocampal and cortical areas. It is relatively less known whether these conclusions apply to the striatal neurons (8).

The striatum, the main input nucleus of the basal ganglia, receives convergent glutamatergic inputs from the cortex and thalamus (9–11). The integration of these functionally distinct inputs is critical for fine movement control and action selection (12, 13). The principal neurons in the striatum—spiny projection neurons (SPNs)—display hyperpolarized membrane potentials (∼−80 mV) at rest, often referred to as the "down-state" (14, 15). It is generally believed that coherent cortical inputs can effectively depolarize SPNs and promote membrane potential transitions from a hyperpolarized down-state to a depolarized "up-state" (∼−55 mV), at which point action potentials can be generated (14–16). To achieve this ∼20- to 30-mV state transition, it has been estimated that a large number (hundreds to thousands) of active inputs would be required (14–17). Interestingly, striatal SPNs are capable of producing long-lasting plateau potentials following activation of spatially clustered and temporally synchronized excitatory inputs at distal dendrites. Such dendritic plateau potentials require much fewer excitatory inputs (tens) and could efficiently promote SPN membrane potential state transitions, representing a unique mechanism for gating the convergent excitatory inputs (8). However, how a dendritic plateau potential integrates subsequent excitatory inputs and shapes the spatiotemporal integration window for generating spike outputs remains unclear.

In addition, the neurons within striatal microcircuits are almost purely inhibitory (18, 19). GABAergic SPNs receive perisomatic inhibition mediated by parvalbumin (PV)-positive fast-spiking (FS) interneurons (20–22), as well as dendritically targeted inhibition from somatostatin (SST)- and neuropeptide Y (NPY)-positive low-threshold spike (LTS) interneurons (23–27) and dendritically targeted collateral inhibition from neighboring SPNs (22, 28, 29). How somatic and dendritic inhibition interacts with nonlinear integration of excitatory inputs in the presence of dendritic plateau potentials remains largely unexplored (30, 31).

Here we investigate how dendritic plateau potentials shape the spatiotemporal integration of both excitatory and inhibitory inputs in striatal SPNs. Experimentally, it is nearly impossible to both achieve precise control of input patterns and monitor membrane potential fluctuations throughout SPNs simultaneously. Therefore, we constructed a detailed SPN model to investigate these phenomena,

Significance

Dendritic plateau potentials generated by the activation of clustered excitatory inputs play a crucial role in neuronal computation and are involved in sensory perception, learning, and memory. Current studies largely focus on the genesis of plateau potentials. However, little is known about how somatic and local dendritic inhibitions control dendritic plateau potentials. The conventional view of the effectiveness of local dendritic inhibition relies on shunting inhibition. Moreover, massive excitatory conductance could overweigh the shunting inhibition. Here we describe a form of cell-type–specific dendritic inhibition in the striatal spiny projection neurons, in which the inhibition provides precise control over the amplitude, kinetics, and duration of plateau potentials, and thus the spiking output of spiny projection neurons.

Author contributions: K.D., Y.-W.W., J.B.D., and J.H.K. designed research; K.D., Y.-W.W., R.L., and Y.L. performed research; J.B.D. and J.H.K. supervised the project; B.R. and G.K. contributed new reagents/analytic tools; K.D., Y.-W.W., and R.L. analyzed data; and K.D., Y.-W.W., J.B.D., and J.H.K. wrote the paper.

Conflict of interest statement: G.K. and B.R. are founders of Femtonics Kft, and B.R. is a member of its scientific advisory board.

This article is a PNAS Direct Submission.

Freely available online through the PNAS open access option.

[1]K.D. and Y.-W.W. contributed equally to this work.

[2]J.B.D. and J.H.K. contributed equally to this work.

[3]To whom correspondence may be addressed. Email: dingjun@stanford.edu or Jeanette.Hellgren@ki.se.

This article contains supporting information online at www.pnas.org/lookup/suppl/doi:10.1073/pnas.1704893114/-/DCSupplemental.

and used experiments to validate key model predictions. Our model predicts that a dendritic plateau potential in SPNs can efficiently broaden both the spatial and temporal integration windows for excitatory inputs, enabling neuron-wide integration for excitation. In contrast, the impact of inhibitory inputs is branch-specific and cell-type–specific. In particular, there is a unique spatiotemporal window for dendritically targeted inhibition to effectively control the duration of a dendritic plateau potential and subsequent spiking. Our model further reveals that the branch-specific inhibition of dendritic nonlinear integration is not primarily attributable to shunting effects of the $GABA_A$ receptor ($GABA_AR$), but through an NMDA receptor (NMDAR) magnesium block (Mg^{2+}-block)–dependent mechanism. Using a combination of electrophysiology, optogenetics, two-photon imaging, and dual-color glutamate (two-photon)/GABA (one-photon) uncaging, we directly demonstrated the spatiotemporal window for the cell-type– and branch-specific inhibition and involvement of NMDAR Mg^{2+} block for inhibition of dendritic plateau potentials. These findings represent a synaptic controlling mechanism for creating a unique spatiotemporal integration window in neurons.

Results

Generation and Propagation of the Dendritic Plateau Potential. We used both experimental and computational approaches to investigate the generation of plateau potentials in SPN dendrites. First, we used combined electrophysiology with two-photon laser-scanning microscopy (2PLSM) and MNI-caged glutamate (MNI-Glu, 5 mM) two-photon laser uncaging (2PLU) to activate clusters of glutamate receptors at the heads of dendritic spines in SPNs (32). We recorded SPNs by using a somatic patch-clamp electrode containing the Alexa Fluor-594 (50 μM) to visualize dendrites. The uncaging laser (730 nm) power was adjusted to evoke excitatory postsynaptic potentials (uncaging-evoked EPSPs; uEPSPs) resembling spontaneous activity (*SI Appendix*, Fig. S1 *A* and *B*). When spatially clustered spines at distal dendrites (>80 μm) were activated within a short temporal window [0.8-ms pulse duration, interstimulus interval (ISI) = 1 ms, 20 spines], such stimulation evoked a prolonged somatic depolarization (plateau potential) lasting tens to hundreds of milliseconds, extending beyond the end of the uncaging pulses. When the same uncaging protocol was applied to proximal dendrites (20–30 μm from the soma), somatic uEPSPs were similar in amplitude, but rapidly decayed immediately after the end of the last uncaging pulse (Fig. 1*A*), consistent with previous report (8). Second, to investigate whether such distally evoked plateau potentials could be generated by intrinsic synaptic release, we placed a theta-glass stimulation pipette adjacent (<5 μm) to a SPN dendrite under visual guidance of 2PLSM (Fig. 1*B*). Similarly, local electrical stimulation (two stimuli at 100 Hz) in the presence of $GABA_AR$ blocker picrotoxin (PTX, 50 μM) could successfully evoke the plateau potentials and the rapidly decayed EPSPs at the distal and proximal dendrites, respectively. Due to the nonselective nature of electrical stimulation, phasic GABA releases could be also triggered by the same stimulation. Therefore, in the absence of PTX, the success rate of generating a plateau potential was extremely low (6.25%, n = 1 of 16 cells). When inhibition was blocked by PTX, the success rate significantly increased (58.3%, n = 7 of 12, Fisher's exact test, P = 0.0042) and the duration of the EPSP was significantly longer [artificial cerebrospinal fluid (ACSF): 36.8 ± 1.9 ms, PTX: 55.0 ± 4.0 ms, Mann–Whitney, P = 0.0028] (*SI Appendix*, Fig. S1 *E–G*), suggesting a tight local inhibitory control on the dendritic plateau potentials.

In parallel, to understand the genesis and propagation of the supralinear membrane potential depolarizations in SPN dendrites, we improved and used a biophysically and morphologically detailed model of the SPN (33, 34) (see also *SI Appendix* for details). The model was equipped with a large array of experimentally verified ion channels (34) (*SI Appendix*, Tables S1–S3). Ion channel kinetics and parameters were tuned to fit the present experimental conditions (*SI Appendix*, Fig. S1) and previously published data (35–37). This is further motivated because SPN dendrites are too thin to be directly accessed using patch-clamp techniques. The SPN model

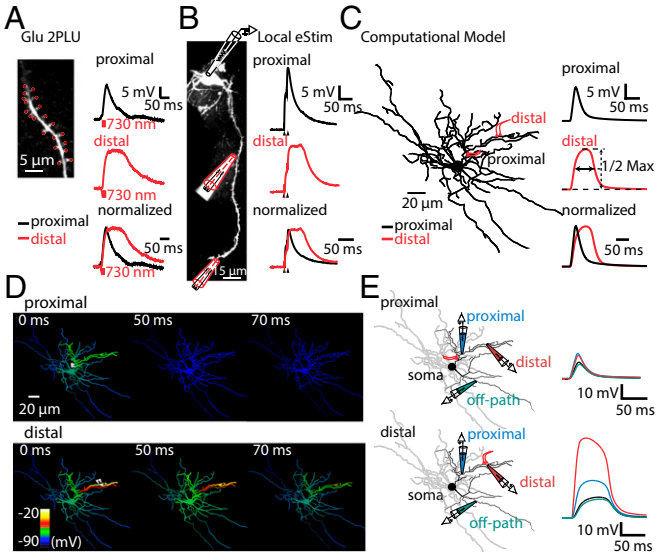

Fig. 1. Propagation of dendritic plateau potential in SPN dendrites. (*A* and *B*) Dendritic plateau potential induced by Glu-2PLU (*A*) or by local electrical stimulation (eStim) (*B*). (*Left*) A representative two-photon image of a SPN dendrite filled with Alexa Fluor-594 (50 μM). Red dots in *A* indicate the locations for glutamate uncaging (730 nm). Local stimulation was achieved by using a theta glass pipette filled with Alexa 594 (5 μM) placed adjacent to the dendrite. (*Right*) EPSPs induced by glutamate uncaging at 20 spines at proximal or distal dendrites, or local eStim in the presence of PTX (50 μM). (*C*) Simulated dendritic plateau potentials in a detailed SPN model. Plateau potential duration was defined as full-width at half-maximum of plateau potentials. (*D*) Simulated membrane potential dynamics throughout dendrites after activation of clustered spines (ISI = 1 ms) at proximal or distal dendrites, as shown in *C*. Membrane potential was visualized using a color map. Arrows indicate the location of clustered spines. "0, 50, 70 ms" indicates the time delay from the activation of the last spine. (*E*) Simulated clustered inputs at proximal (*Upper*) and distal (*Lower*) dendrites result in membrane potential fluctuations in the distal (red), the proximal (blue) compartments of the input dendrite, in the soma (black), or in the noninput dendrite (off-path, green).

faithfully reproduces SPN intrinsic membrane properties (*SI Appendix*, Fig. S1 *C* and *D*) (35–37). In addition, when we simulate somatic membrane potential fluctuations in response to activation of 15 spines (ISI = 1 ms) at distal but not proximal dendrites, a plateau potential can be elicited (Fig. 1*C*). The amplitude and duration of the simulated somatic depolarization closely recapitulated our experimental data (Fig. 1 *A* and *B*). We then visualized membrane potential fluctuations of the whole SPN while activating clustered spines placed either in a distal or a proximal dendritic branch (Fig. 1*D* and Movie S1). The model showed that clustered activation of spines in the distal dendrite powerfully depolarized the branch up to ~−20 mV (Fig. 1*D*). We monitored the local dendritic membrane potentials at different locations: "distal-input site," "proximal-input site," and "off path" (at a noninput dendrite), as well as the somatic membrane potentials (Fig. 1*E*). Such a dendritic plateau potential in the "hot" branch could persistently fuel depolarization, and eventually propagated and caused a long-lasting depolarization spreading to the soma and noninput dendrites. This finding was also consistent with our experimental observations.

Dendritic Plateau Potentials Broaden the Spatiotemporal Window for Integrating Excitatory Inputs. Dendritic plateau potentials could efficiently propagate and cause a sustained depolarization throughout the model SPN. The presence of sustained and widespread depolarizations implies that the spatiotemporal window for integrating the subsequent excitatory inputs could be broadened in the SPN. To test this, we generated a dendritic plateau potential by activating the clustered excitatory inputs within a short time window using the

model SPN. Then a group of 20 synapses, in addition to spontaneous synaptic background noise, were randomly distributed in the dendrites and each synapse activated independently with high-frequency activity (10 Hz in a Poisson distribution) to mimic cortical activity (38). To avoid potential biases on the spatial locations of the synapses, which may perturb statistics, we generated a large sample pool with 1,000 unbiased distribution patterns (Fig. 2*A* and Movie S2). Spontaneous synaptic activity or high-frequency inputs alone only caused a mild depolarization (2–6 mV) and failed to elicit action potentials. When a dendritic plateau potential was generated by distal clustered inputs and high-frequency inputs were concurrently activated ($\Delta t_{Ext} = 0$ ms), the firing probability in the model SPN was ~80%. Firing probability was much lower when using the same activity patterns but with the clustered inputs placed proximally (~3%). To investigate the temporal integration window, we varied the timing between the clustered inputs and the high-frequency inputs with a delay of Δt_{Ext}. When the high-frequency inputs were delayed following the clustered inputs, the firing probability decreased. When the delay was longer than 10 ms, the probability of firing an action potential dropped down to nearly zero. In contrast, the firing probability remained ~35% with $\Delta t_{Ext} = 50$ ms when a dendritic plateau potential was generated using clustered inputs distally (Fig. 2*B*). The relationship between the firing probability and the delay between the clustered inputs and the high-frequency inputs (Δt_{Ext}) showed a distinct temporal integration window (Fig. 2*C* and *SI Appendix*, Fig. S2 *A* and *B*). Furthermore, the broadening of the temporal integration window cannot fully be explained by somatic depolarization (*SI Appendix*, Fig. S2 *C* and *D*). These data suggest that dendritic plateau potentials generated by activation of distally clustered spines can significantly enhance the SPN's capacity to integrate temporally delayed excitatory inputs and broaden the "reading window" to even incorporate temporally separated information.

To determine whether dendritic plateau potentials could integrate excitatory inputs with different spatial distribution profiles, we analyzed the relationship between the firing probability and the average location of 20 high-frequency activated synapses (Fig. 2*D*). As expected, because of dendritic filtering, the membrane potential depolarizations were slightly bigger when the high-frequency inputs were placed proximally (*SI Appendix*, Fig. S2*E*). However, when coupling these high-frequency activated synapses with the dendritic plateau potential, the exact location of the 20 synapses had little effect on the spiking probability (Fig. 2*E* and *SI Appendix*, Fig. S2*F*). Together, these data suggest that a dendritic plateau potential could broaden the spatiotemporal integration of excitatory inputs to SPNs.

Model Predicts a Unique Spatiotemporal Window for Cell-Type–Specific Inhibition. In addition to receiving massive excitatory inputs from external sources, SPN dendrites are heavily innervated by various types of intrastriatal inhibitory inputs (18, 19, 27). We therefore tested how the synaptic integration mechanism is fine-tuned by inhibition. We simulated the model with clustered inputs at a distal dendrite, synaptic background noise, high-frequency excitatory inputs, and in addition we added inhibitory inputs at different locations (Fig. 3*A*). To model the inhibition generated by the striatal inhibitory microcircuits, we modified the channel kinetics of unitary GABAergic synaptic conductances to mimic different inhibitory inputs (Fig. 3*B*) (18, 19): (*i*) FS-mediated perisomatic inhibition (FS GABA), (*ii*) SPN and LTS interneuron-mediated dendritic inhibition with fast kinetics (fast GABA), and (*iii*) NPY-expressing neurogilaform (NPY-NGF) interneuron-mediated dendritic inhibition with slow kinetics (slow GABA) (26, 39, 40). We first monitored the membrane potential perturbations (ΔVm) caused by inhibition with different delay timing (Δt_{Inh}) on plateau potentials (Fig. 3*C*). The dendritic slow and fast GABA inputs both caused large membrane potential perturbation measured at the soma, whereas the somatic FS GABA inputs only generated small ΔVm. Interestingly, dendritic and somatic inhibitions generated distinct temporal profiles of ΔVm (Fig. 3*C*). To further test how ΔVm translates into inhibitory effects on spiking, concurrent activation of the clustered and high-frequency inputs was used to trigger action potentials with an initial firing probability of ~80% (Fig. 3*D*). Similarly, unitary somatic FS GABA inhibition had little effect on spiking probability, regardless of timing. In contrast, dendritic slow GABA inhibition shut down spiking very effectively with a broad temporal window (Fig. 3*D* and Movie S3). Interestingly, the dendritic fast GABA—the majority of striatal inhibitory synapses (18)—only effectively inhibited spiking in a narrower temporal window (Fig. 3*D*). For example, the unitary fast GABA inhibition near the plateau potential initiation zone caused a significantly decrease in firing probability when Δt_{Inh} was larger than 20 ms, and peaked around 40–60 ms.

To compare the impact of the dendritic fast inhibition with somatic inhibition in a near physiological condition, we generated a spiking pattern for FS interneurons by inserting 20 FS GABA synapses (G_{max} = 1,500 pS) into the perisomatic region, each of which received high-frequency drive (30 Hz, Poisson trains with short-term depression) (28). We performed simulations with fixed Δt_{Inh} coupled with different Δt_{Ext} (Fig. 3*E*). The simulation showed that somatic FS inhibition impacted firing with a much narrower time window even though inhibitory postsynaptic currents (IPSCs) lasted for over 100 ms (Fig. 3*E*, *Inset*). Next, to further test the spatial sensitivity of dendritic fast inhibition in a more physiological condition, we generated a group of random inhibitory input patterns (20 synapses, G_{max} = 1,500 pS, Poisson train at 5 Hz for

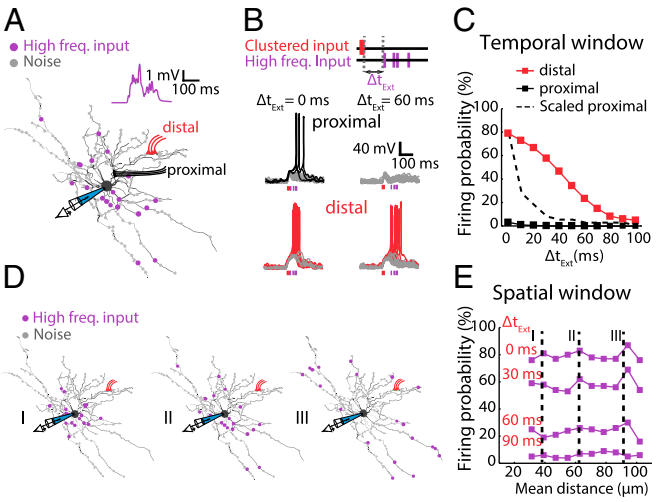

Fig. 2. Dendritic plateau potentials broaden the spatiotemporal integration window for excitatory inputs. (*A*) The SPN model was loaded with background Poisson noise (small gray dots), which include randomly distributed excitatory and inhibitory synapses. Clustered inputs were added either at distal (red) or proximal (black) dendrites. In addition to the clustered input and the background noise, a group of 20 excitatory synapses (uEPSP = ~0.6 mV) were randomly distributed in the dendrites (purple dots), with each synapse receiving an independent Poisson train of inputs at 10-Hz frequency for 200 ms (termed as "High freq. input" throughout the figures). The spatial and temporal pattern for the Poisson trains varied in each simulation trial. (*Inset*) A representative trace of somatic membrane potentials during a single trial (also see *SI Appendix*, Fig. S2). (*B*) Triggered activities when pairing clustered and high-frequency inputs. (*Upper*) Simulated inputs pattern. (*Lower*) Sample traces of modeled somatic membrane potential fluctuations or spiking. Gray traces indicate that no action potential was triggered. (*C*) The firing probability resulting from high-frequency inputs as a function of the time delay between the clustered inputs and high-frequency inputs (Δt_{Ext}). Clustered inputs were provided either distally (red) or proximally (black) as indicated in *A*. For comparison, the dashed line indicates the scaled firing probability of pairing high-frequency inputs with proximally evoked plateau potential. Distally evoked dendritic plateau potentials broadened the temporal integration window for excitatory inputs. (*D*) Representative examples showing randomly generated spatial patterns for high-frequency inputs, described as: proximal (I), medial (II), and distal (III) inputs. (*E*) The firing probability of dendritic plateau potentials coupled with high-frequency inputs starting at different Δt_{Ext} was plotted as a function of mean distance from the soma. Dashed lines indicate the mean distance-to-soma of inputs shown in *D*. Even though the mean distances were different, there was a cell-wide integration dependent mainly on Δt_{Ext}.

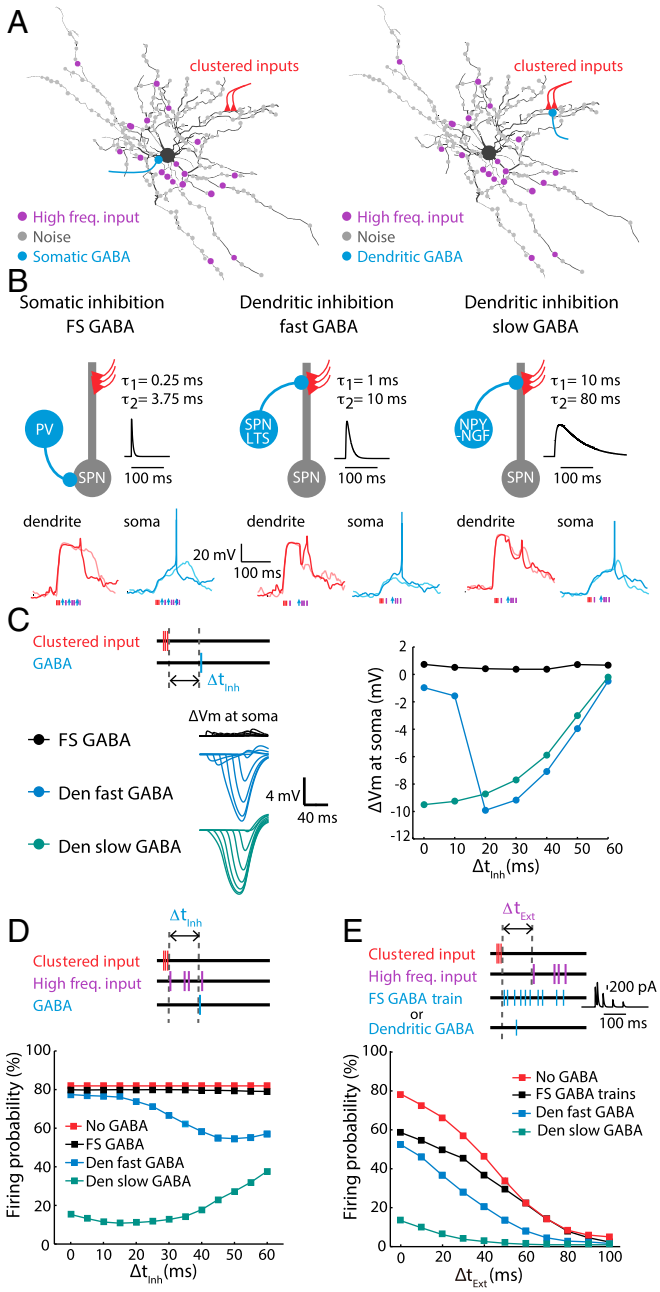

Fig. 3. Perisomatic and dendritic inhibition of spiking. (*A*) The simulation scheme for clustered, high-frequency excitatory and inhibitory inputs. In addition to background noise and high-frequency inputs, the model SPN was loaded with additional inhibitory inputs either placed at the perisomatic region or dendritic locations near the site for generating plateau potentials. (*B*) Illustrations of three major types of inhibition onto striatal SPNs: (*i*) perisomatic inhibition by PV-positive FS interneurons (FS GABA, *Left*), (*ii*) dendritic targeting inhibition with fast kinetics resembling SPN or LTS inputs (fast GABA, *Center*), and (*iii*) dendritic targeting inhibition with slow kinetics resembling NPY-NGF inputs (slow GABA, *Right*). (*Insets*) Examples of simulated voltage traces (two trials, spiking and nonspiking) at the soma (blue curves) and the plateau site (red curves). (*C*, *Upper Left*) Schematic for simulation. Membrane potential perturbation (ΔVm) was obtained via subtraction of plateau potentials with and without inhibition. (*Lower Left*) Representative traces of somatic ΔVm at different time of onset (Δt_{Inh}). (*Right*) Peak amplitudes of ΔVm were plotted as a function of Δt_{Inh}. (*D*) The effect of the timing of perisomatic (FS GABA) and dendritic inhibition on firing probability. Clustered and high-frequency excitatory inputs were followed by different types of GABAergic inhibition with varied time of onset (Δt_{Inh}). (*E*) The effect of different types of inhibition patterns on the temporal integration of excitation. Firing probability is plotted as function of the onset of the high-frequency input (Δt_{Ext}), with fixed timing for FS GABA trains or dendritic inhibition.

200 ms) with three types of distributions (sample size $n = 1{,}000$) (*SI Appendix*, Fig. S3 *A* and *B*): (*i*) distributed over the distal dendrites (distal), (*ii*) distributed over the proximal dendrites (proximal), and (*iii*) distributed only on the input branch where the clustered spines were activated (in branch). The model showed that either distal or proximal global inhibition weakly inhibited spiking, whereas placing inhibitory synapses in branch was more effective in preventing spiking (*SI Appendix*, Fig. S3 *C* and *D*). Nevertheless, the on-site unitary inhibitory input at the optimal timing was still 10 times more efficient than in-branch inhibition (*SI Appendix*, Fig. S3 *C* and *D*): 2 inhibitory synapses on-site had a nearly equivalent effect on spiking compared with 20 inhibitory synapses activated at 5 Hz for 200 ms in branch.

Could this temporal window for the fast GABA inhibition be observed at different dendritic locations (41)? To address this question, the unitary fast GABA synapse was placed at: (*i*) the distal dendrite where clustered inputs were activated (on-site) (42), (*ii*) proximally in the activated dendrite (on-path) (43), (*iii*) the perisomatic region (soma) (39), and (*iv*) the neighboring dendrite (off-path). Similar to previous simulation schemes, we varied the Δt_{Inh} and found that somatic or off-path inhibition had little effect on firing probabilities (*SI Appendix*, Fig. S4 *A* and *B*). Inhibition on-path had a considerable effect but was much weaker compared with inhibition on-site. However, neither the perisomatic, off-path, nor the on-path inhibition exhibited temporal profiles similar to on-site inhibition. In addition, temporal windows for on-site inhibition were still present with varied Δt_{Ext} (0, 30, and 60 ms) or with different E_{Cl^-} (−60 to −75 mV) (*SI Appendix*, Fig. S4 *C* and *D*). One mechanism that might account for such different temporal profiles could be the different driving forces of Cl^-, because dendritic membrane potentials were more depolarized at the clustered input site (Fig. 1*E*). To directly address this in our model SPN, we replaced unitary inhibitory conductances with current injections mimicking GABAergic IPSCs. Similarly, on-site current injections had the strongest impact on firing probability (*SI Appendix*, Fig. S4 *E* and *F*), suggesting that the different driving forces for Cl^- do not account for the location-specific inhibition.

Taking these data together, our model revealed a dendritic branch-specific inhibition as a mechanism for controlling SPN synaptic integration. This dendritic inhibition could be potentially mediated by different types of interneurons or by neighboring SPNs. It is interesting that even though the model maximal conductance (G_{max}) for FS GABA, dendritic fast GABA, and slow GABA synapses is the same, the efficacy on inhibiting spiking is very different: FS-like unitary GABA synapses had very little effect; dendritic fast GABAergic synapses could prevent spiking with intermediate efficacy at optimal timing; and dendritic slow GABA IPSCs most efficiently attenuated spiking activity with a broad temporal window. Local dendritic inhibition (on site or in branch) has a unique temporal profile, suggesting the existence of an optimal temporal window for silencing spike output.

Critical Timing for Dendritic Inhibition. Our simulation data suggested the existence of an optimal temporal window for attenuating dendritic plateau potentials. To directly test this, we used optogenetic tools to selectively activate perisomatically and dendritically targeted inhibition. To achieve cell-type–specific expression of channelrhodopsin-2 (ChR2), we injected adeno-associated virus (AAV-DIO-ChR2-mCherry) into the dorsolateral striatum of PV-Cre or A2a-Cre mice to express ChR2 in FS interneurons and indirect pathway SPNs (iSPNs), respectively (*SI Appendix*, Fig. S5 *A*–*C*). Blue laser illumination (focal diameter: ∼19 μm) was used to trigger GABA release from ChR2-expressing axonal terminals (*SI Appendix*, Fig. S5 *D* and *G*). A common approach for generating a dendritic plateau potential is near-simultaneous activation of a

group of spatially clustered excitatory inputs using glutamate 2PLU. However, the most commonly used glutamate caged compound for 2PLU, MNI-Glu, is a $GABA_AR$ antagonist (44), which would prevent us from studying the role of $GABA_AR$ in the genesis and function of dendritic plateau potentials. Therefore, we used 4-methoxy-5,7-dinitroindolinyl-L-glutamate trifluoroacetate (DNI-caged glutamate, DNI-Glu, 0.7 mM), which has been demonstrated to exhibit ∼seven times more potency to the same concentration of MNI-Glu (45), without completely blocking $GABA_ARs$ [preserving ∼40% of the peak amplitude of optogenetically induced IPSC (oIPSC)] (*SI Appendix*, Fig. S5*E*). The intensities of the laser powers used for 2PLU and optogenetic stimulation were tuned to make sure the amplitude and waveforms of uEPSPs were comparable to spontaneous EPSPs (*SI Appendix*, Fig. S1*A*), and ratios between oIPSC and uEPSC amplitudes resembled those obtained with local electrical stimulation (Fig. 4*A* and *SI Appendix*, Fig. S5*F*).

We first recorded and visualized the dendrites of ChR2 nonexpressing direct-pathway SPNs (dSPNs) in A2a-Cre mice 4–6 wk after AAV-DIO-ChR2-mCherry injections (*SI Appendix*, Fig. S5*A*). We then evoked GABA release from dendritically targeted iSPN axon terminals after activating clustered dendritic spines at a distal dendrite with DNI-Glu-2PLU (Fig. 4 *A* and *B*). Using the same recording conditions (Fig. 1*A*), plateau potentials (mean half-duration: 86 ± 5 ms, $n = 15$) were readily and repeatedly induced (Fig. 4*C*). When optogenetic stimulation was paired with DNI-Glu-2PLU at different timing (Δt_{Inh} = 10, 30, 50, and 70 ms), we observed a clear hyperpolarizing deflection of the plateau potentials caused by dendritic inhibition from iSPN (Fig. 4*C*). We quantified the peak amplitude of ΔVm by subtracting the membrane potentials recorded with (Fig. 4*C*, red) and without (Fig. 4*C*, black) optogenetic stimulations, and $\Delta area$, the area-under-curve of ΔVm (Fig. 4*D*). Remarkably, the ΔVm and $\Delta area$ caused by inhibition 30 ms after the induction of dendritic plateau potential (Δt_{Inh} = 30 ms) was significant larger than those obtained by the same stimulation with different temporal delays (Δt_{Inh} = 10, 50, and 70 ms). These data confirmed our modeling results, which predicted the existence of a preferred temporal window for dendritic inhibition on plateau potentials [ΔVm (Δt_{Inh}) = −2.9 ± 0.4 mV (10 ms), −4.3 ± 0.5 mV (30 ms), −2.5 ± 0.5 mV (50 ms), −2.1 ± 0.3 mV (70 ms), n = 15, $P < 0.0001$; $\Delta area$ (Δt_{Inh}) = −141 ± 23 mV × ms (10 ms), −233 ± 23 mV × ms (30 ms), −128 ± 28 mV × ms (50 ms), −93 ± 22 mV × ms (70 ms), $n = 15$, $P < 0.0001$, Friedman test followed by Dunn's multiple comparisons test] (Fig. 4 *D–F*).

Next, we performed analogous experiments: recording SPNs in PV-Cre mice after ChR2 expression. We activated axon terminals of PV neurons at perisomatic regions to examine the impact of perisomatic inhibition on plateau potentials (Fig. 4 *G–I*). Similar to results obtained from A2a-Cre mice, oIPSCs or hyperpolarizing membrane potential perturbations (Fig. 4 *G–I*) were observed when GABA release was triggered by blue laser stimulation. In contrast, when inhibition was evoked at perisomatic regions, we did not observe a preferred temporal window for inhibition [ΔVm (Δt_{Inh}): −2.6 ± 0.4 mV (10 ms), −2.6 ± 0.3 mV (30 ms), −2.5 ± 0.3 mV

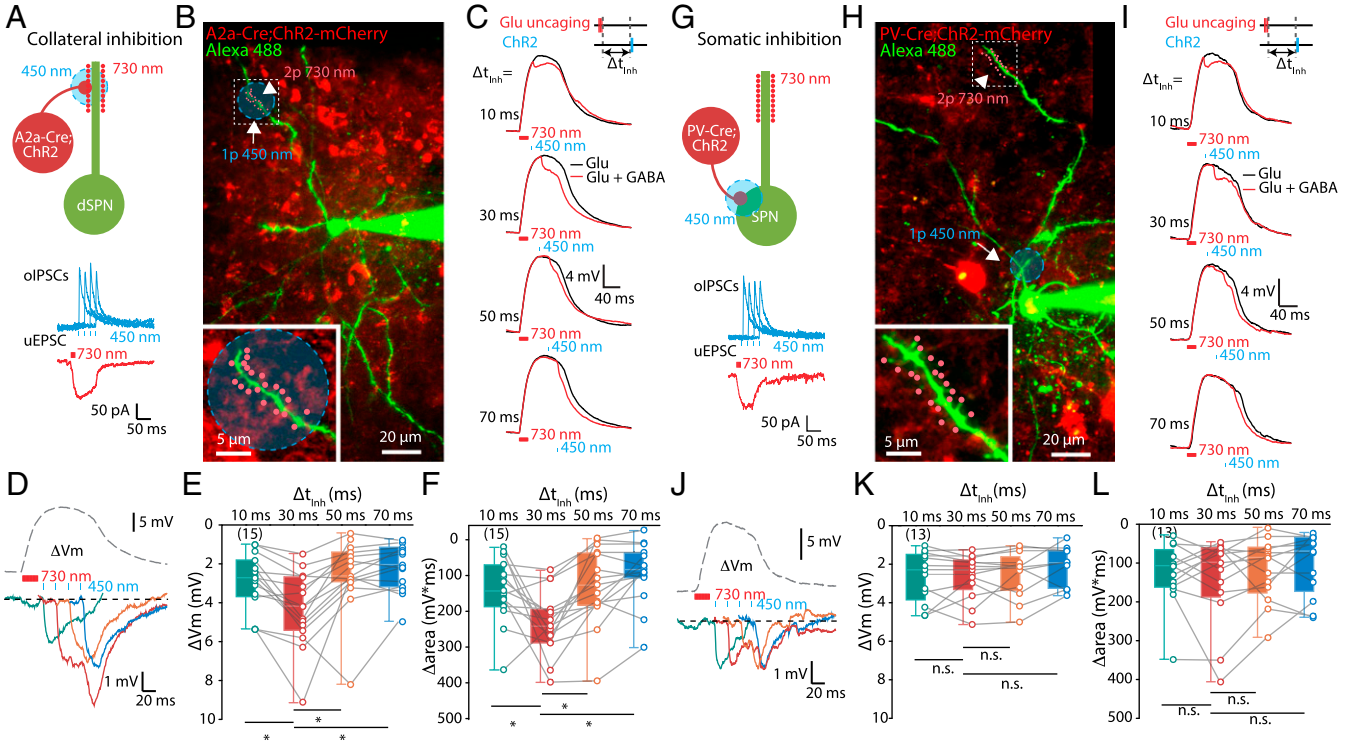

Fig. 4. Inhibition of dendritic plateau potential by SPNs and PV-positive interneurons. (*A*) Dendritic inhibition of plateau potentials by SPN-mediated collateral inhibition. (*Upper*) Experimental scheme of dendritic collateral inhibition on plateau potential in dSPNs by A2a-Cre expressing iSPNs. (*Lower*) The representative traces of oIPSCs (blue) of collateral inhibition by iSPNs and uEPSC (red) for plateau potential induction. (*B*) Two-photon image of a dSPN (green) in a brain slice with ChR2-mCherry (red) expression from A2a-Cre mice. The 720-nm and 450-nm laser locations for 2PLU (arrowhead) and optogenetic stimulation (arrow) are marked as red spots and blue circle, respectively. (*C*) Representative traces of plateau potential without (black) and with (red) dendritic collateral inhibition by SPNs at four different Δt_{Inh} (10, 30, 50, and 70 ms). (*D*) Representative traces for ΔVm aligned with the trace of plateau potential. (*E* and *F*) Summary result of dendritic collateral inhibition of plateau potential by SPNs. ΔVm and $\Delta area$ were significant larger at $\Delta t_{Inh} = 30$ ms ($P < 0.0001$ for both). (*G*) Somatic inhibition of plateau potentials by PV interneuron-mediated inhibition. (*Upper*) Same as in *A* but the 450-nm laser was illuminated at perisomatic region. (*Lower*) Same as in *A* but oIPSCs were mediated by somatic inputs of PV interneurons. (*H*) Two-photon image of a SPN (green) in a brain slice with ChR2-mCherry (red) expression from PV-Cre mice. Red spots and blue circle indicate locations for 2PLU (arrowhead) and optogenetic stimulation (arrow), respectively. (*I* and *J*) Same as in *C* and *D* but the ΔVm was mediated by perisomatic inhibition of PV interneurons. (*K* and *L*) Summary result of somatic inhibition of plateau potential by PV interneurons. No significant difference in ΔVm ($P = 0.1199$) and $\Delta area$ ($P = 0.2781$) were observed between different Δt_{Inh}. *$P < 0.05$; n.s., no significant difference.

(50 ms), −2.1 ± 0.3 mV (70 ms), $n = 13$, $P = 0.1199$; $\Delta area$ (Δt_{Inh}) = −126 ± 23 mV × ms (10 ms), −143 ± 32 mV × ms (30 ms), −117 ± 23 mV × ms (50 ms), −100 ± 22 mV × ms (70 ms), $n = 15$, $P = 0.2781$, Friedman test followed by Dunn's multiple comparisons test] (Fig. 4 *J–L*), which is in agreement with our simulation data (Fig. 3*C*). It is worth noting that recruiting sparse and dendritic targeting PV axon terminals (with stronger blue laser stimulation at the dendrite), we found a similar optimal temporal window of inhibition as in A2a-Cre mice (*SI Appendix*, Fig. S5 *G–K*), suggesting the location of the inhibitory synapse is the deterministic factor.

Together, these data demonstrated that dendritically targeted inhibition can effectively modulate plateau potentials within a confined spatiotemporal window, and thus directly support our simulation results. Although sparser and weaker compared with perisomatic FS interneuron to SPN synapses, dendritically targeted inhibitory inputs could effectively modulate SPN spiking output by modulating local nonlinear synaptic integration in SPN dendrites.

Mechanism for Effective Inhibitory Control of Dendritic Plateaus. What mechanisms could account for different efficacies for dendritic inhibition at different time points following plateau potentials? If assuming that GABAergic inputs have the same maximum conductance, the inhibitory efficacy could be determined by both driving force and local input resistance. Our simulation using constant current injections (*SI Appendix*, Fig. S4 *E* and *F*) suggested that driving force alone could not account for the high efficacy of local dendritic inhibition. Therefore, we focus on the influence of local input resistance. Dendritic input resistance is a fundamental parameter that determines the local responsiveness to synaptic input (46). To capture the fine details of dendritic responsiveness, we examined the transient-state of the dendritic membrane potential perturbations (ΔV) in response to short excitatory (depolarizing) and inhibitory (hyperpolarizing) inputs using our model SPN.

We injected either depolarized or hyperpolarized current test pulses (2- to 20-ms duration, 20 pA) and shifted the timing of current injection. The ΔV was measured at the location where the clustered spines are activated (Fig. 5*A*). Strikingly, we found that when the plateau potential was evoked, the dendrite responded differentially to depolarized and hyperpolarized pulses, and the absolute value of peak ΔV ($|\Delta V|$) displayed asymmetric responsive curves to external stimuli: the peak $|\Delta V|$ caused by hyperpolarized pulses rose before those caused by depolarized pulses (Fig. 5 *B* and *C*). The ratio between excitatory $|\Delta V|$ and inhibitory $|\Delta V|$ (defined as the E/I ratio) follows a biphasic distribution, which evolves with the simulation time (Δt): the ratio peaks at 0.2 and 1.8 at two phases, indicating the balance shifted from inhibition to excitation (Fig. 5*D*). The biphasic distribution of E/I suggested a temporal window favoring local inhibition peaked at ∼30–50 ms after the last clustered excitatory input (Fig. 5*E*). This temporal window is consistent with our simulation examining ΔVm and spiking probability (Fig. 3 *C* and *D*). It is worth noting that the asymmetry E/I ratio is correlated to amplitudes and locations. In the clustered input branch, the amplitudes of dual phase are strongest. As the location gradually shifts away from the plateau potential origin to the soma, such phenomena faded out (Fig. 5*F* and *SI Appendix*, Fig. S6).

What is the mechanism for the biphasic E/I ratio in the local dendrite after a dendritic plateau potential is generated? The responsiveness of the neuron is determined by its intrinsic and synaptic properties, for example, calcium channels (8), A-type potassium channels (KA), and inward-rectifying potassium channels (Kir) (34). To assess the contribution of ion channels to the dendritic plateau potential, we simulated dendritic voltage-clamp experiments with the voltage command given in the form of a plateau potential. The currents contributed by individual ion channels during the dendritic plateau potential were isolated (*SI Appendix*, Fig. S7 *A–C*). We found that the plateau potential duration could be modulated by various transient ionic currents. For example, blocking KA and Kir could significantly prolong the duration of the plateau potential (*SI Appendix*, Fig. S7*D*). Although the shape of the plateau potential was dramatically changed by removing active conductances, the biphasic E/I curve was still prominent in the local compartment (*SI Appendix*, Fig. S7*D*), suggesting that local active conductances could only modulate the shape of dendritic plateau potentials but did not account for the biphasic E/I curve.

In addition to voltage-gated ion channels, NMDAR-mediated currents are critical for plateau potential generation (*SI Appendix*, Fig. S8) and dendritic nonlinearity. Because the only nonlinear variable for NMDAR function with regard to membrane voltage is the function of Mg^{2+} block, we speculate that voltage-sensitive Mg^{2+} block may be important for determining local dendritic responsiveness and the biphasic E/I curve. To rule out contributions by other active conductances, the plateau potential induction was repeated in a purely passive SPN model (Fig. 6*A*). We found that dendritic plateau potentials were still readily induced by 10–20 activated spines, and the biphasic E/I curve was still observed (Fig. 6*B*). Interestingly, in all simulated conditions, the balanced point—where the E/I ratio equals 1—appeared to be at a near-fixed membrane potential at the falling phase of the plateau potential (indicated by

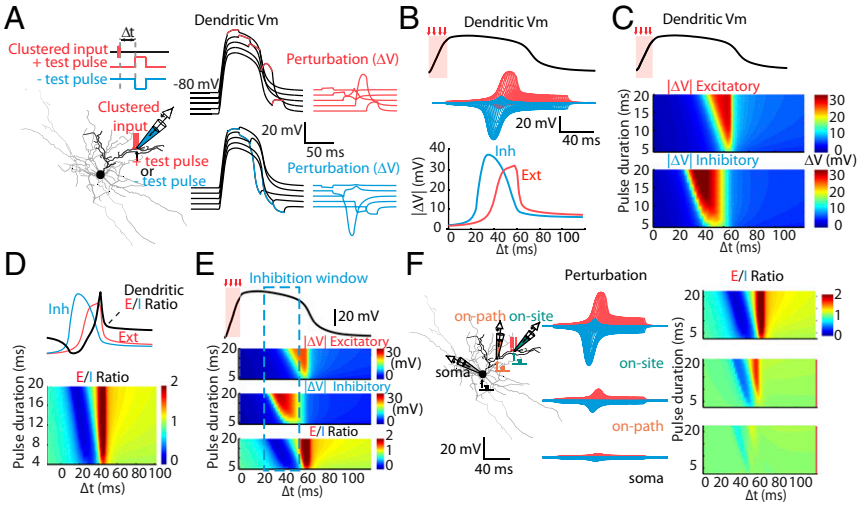

Fig. 5. Asymmetric temporal windows of membrane potential perturbation. (*A*) Schematics for simulation of membrane potential perturbations ($|\Delta V|$) in response to a short current injection (test pulse). (*Left*) A dendritic plateau potential was induced by activation of distal clustered inputs. Current injection and local membrane potential measurements were achieved by a simulated local patch clamp electrode. (*Center*) Example traces of local dendritic membrane potential fluctuation in response to test-pulse current injections: +20 pA (*red*) or −20 pA (*blue*) for 20 ms with varied timing (Δt). (*Right*) Subtracted traces of membrane potential perturbation. (*B*, *Upper*) Membrane potential of a dendritic plateau potential. Red shaded area indicates the timing of clustered inputs. (*Center*) Membrane potentials perturbations evoked by positive (red curves) or negative (blue curves) test pulses with different timings were aligned, showing asymmetry in their distributions. (*Lower*) Peak amplitude of $|\Delta V|$ plotted as a function of Δt. (*C*) Summary results of $|\Delta V|$ obtained with varied durations of test pulses (2–20 ms), visualized with color maps. (*D*, *Upper*) the ratio of excitatory and inhibitory peak $|\Delta V|$ (E/I ratio) were obtained by dividing excitatory and inhibitory $|\Delta V|$. (*Lower*) The E/I ratio as a function of test pulse timing (Δt) and duration (2–20 ms); same as in *C*. (*E*) Aligning dendritic membrane potential, excitatory and inhibitory $|\Delta V|$ (from *C*), and E/I ratio (from *D*) revealed a temporal window favoring inhibition (dashed window frame). (*F*) Spatial profiles of the E/I ratio at selected locations (on-site, on-path, and at the soma). Note that the biphasic E/I ratio was most prominent in the on-site location.

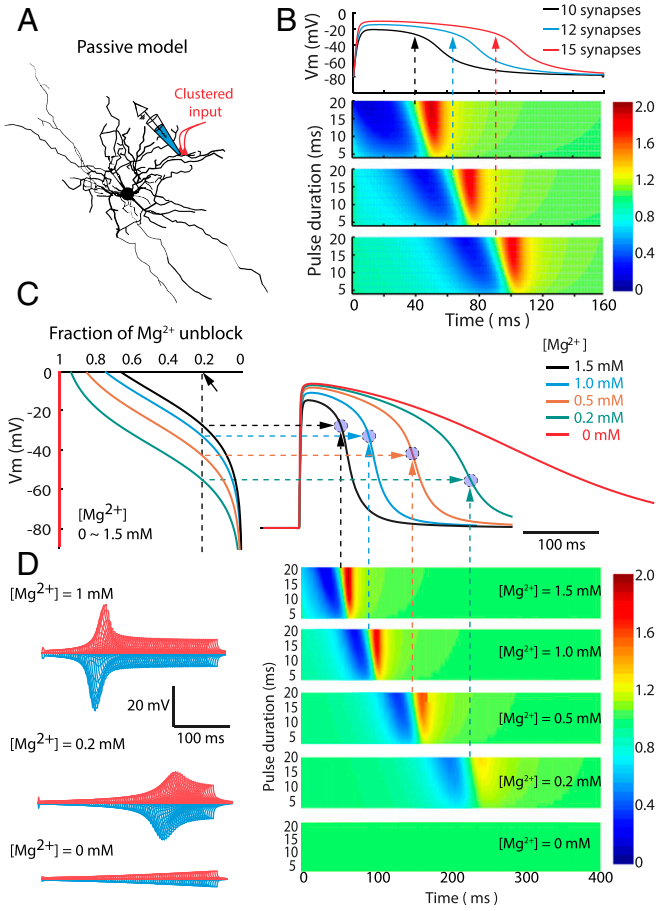

Fig. 6. Magnesium block of NMDAR determines the biphasic E/I ratio. (*A*) Dendritic plateau potentials generated in a pure passive model. (*B*, *Upper*) Sample traces of dendritic plateau potential induced by 10, 12, and 15 synapses, respectively. The simulated voltage traces were recorded from the same compartment as the clustered input. (*Lower*) E/I ratio in the passive model. The heat-maps represent E/I ratio as a function of test pulse timing (Δt) and duration (2–20 ms) induced by 10, 12, and 15 synapses, respectively. Arrows indicate the balanced point where the ratio of E/I was ~1. (*C*) Effects of extracellular Mg^{2+} concentration ($[Mg^{2+}]$) on dendritic plateau potentials. (*Left*) Fraction of Mg^{2+}-unblock. (*Right*) Sample traces of the plateau potential induced by 15 synapses with different $[Mg^{2+}]$. (*D*) Effects of $[Mg^{2+}]$ on the E/I ratio. (*Left*) Sample traces of excitatory and inhibitory $|\Delta V|$ with different $[Mg^{2+}]$. (*Right*) Heat-maps show E/I ratios under different $[Mg^{2+}]$. Note that the strength of the biphasic E/I ratio faded when $[Mg^{2+}]$ approached 0 mM. In Mg^{2+}-free situation, the biphasic phenomenon vanished. The balance points (defined by E/I ratio = 1) could be predicted by ~20% Mg^{2+}-unblock in different $[Mg^{2+}]$ conditions.

arrows in Fig. 6*B*). Next, we manipulated the efficacy of the Mg^{2+} block by simulating dendritic plateau potentials with different extracellular Mg^{2+} concentrations ($[Mg^{2+}]$) (Fig. 6*C*). The duration and the abrupt falling kinetics of dendritic plateau potentials were drastically prolonged by reducing $[Mg^{2+}]$. Furthermore, the color-coded biphasic E/I response curves faded with lowered $[Mg^{2+}]$ (Fig. 6*D*). In Mg^{2+}-free conditions, the biphasic E/I curve completely vanished (Fig. 6*D*). Interestingly, in various $[Mg^{2+}]$ simulation conditions, the calculated balance points do not appear to be at fixed membrane potentials; rather, the balance points appeared to be near a fixed fraction of Mg^{2+} unblock. These simulation results suggest that after the dendritic plateau potential is generated, the Mg^{2+} block of NMDARs is the determining factor for dendritic inhibition. Membrane potential repolarization caused by local dendritic inhibition could re-establish the Mg^{2+} block of NMDARs, which would further attenuate local membrane potential, accounting for branch-specific inhibition and biphasic E/I response curves.

Mg^{2+} Block and Inhibition of Dendritic Plateau Potentials. Our simulation predicted that Mg^{2+} block of NMDARs is critical for inhibitory control of dendritic plateau potential within the same dendritic compartment in SPNs. Activation of NMDARs is required for generation of dendritic plateau potentials. We confirmed this finding by using local stimulation in acute brain slice. The successfully induced plateau potentials in the presence of PTX could be attenuated by MK-801 (10 μM), an NMDAR blocker ($P = 0.0313$) (*SI Appendix*, Fig. S8). These data are consistent with a previous report (8) and suggest that the generation of a dendritic plateau potential requires blockage of local inhibition and activation of NMDARs (47, 48).

We next performed ex vivo slice experiments to verify the involvement of the Mg^{2+} block of NMDARs in branch-specific inhibition. To gain precise control over both excitatory and inhibitory input patterns, we used dual-color GABA (one-photon) and glutamate 2PLU. This was achieved by using Rubi-GABA (20 μM) with blue light illumination (450 nm, 5–10 ms) (*SI Appendix*, Fig. S9*A*). GABA uncaging-induced IPSCs (uIPSCs) were not sensitive to $GABA_B$ receptor antagonist (CGP 55845, 10 μM) and were completely blocked by PTX (50 μM) (*SI Appendix*, Fig. S9*B*). Glutamate uncaging was achieved by using 2PLU of DNI-Glu (0.7 mM) (Fig. 7*A*). DNI-Glu only mildly inhibits the uIPSCs at this concentration (~34%) (*SI Appendix*, Fig. S9 *C* and *D*). The uncaging laser powers were tuned to make sure that amplitude and waveforms of uEPSPs were comparable to spontaneous EPSPs (*SI Appendix*, Fig. S1*B*), and ratios between uIPSCs and the plateau potential triggering uEPSCs resembled those obtained with local electrical stimulation (*SI Appendix*, Figs. S5*F* and S9*E*).

DNI-Glu-2PLU at the heads of a cluster of spines along the distal dendrite generated a dendritic plateau potential (Fig. 7*A*). When DNI-Glu-2PLU was coupled with GABA uncaging at the same location (on branch) with a delay of 20 ms, activation of $GABA_A$Rs efficiently shut down the plateau potential. In contrast, when GABA uncaging was applied at the perisomatic region (perisomatic) with the same stimulation protocol, the plateau potential was only slightly reduced in peak amplitude without change in duration (Δ*duration*: on branch: 34 ± 1%, $n = 7$; perisomatic: 1 ± 2%, $n = 7$, Mann–Whitney, $P = 0.0006$) (Fig. 7 *B* and *C*). Whereas both uncaging protocols caused similar reductions in peak amplitudes of the plateau potentials (on branch: 91 ± 3%, $n = 7$; perisomatic: 93 ± 5%, $n = 7$, Mann–Whitney, $P = 0.7104$) (Fig. 7 *B* and *C*), on-branch GABA uncaging elicited larger Δ*Vm* and Δ*area* compared with the same uncaging applied to perisomatic locations (Δ*Vm*: on branch: 5.1 ± 0.6 mV, $n = 7$; perisomatic: 0.8 ± 0.3 mV, $n = 7$, Mann–Whitney, $P = 0.006$; Δ*area*: on branch: 573 ± 117 mV × ms, $n = 7$; perisomatic: −78 ± 116 mV × ms, $n = 7$, Mann–Whitney, $P = 0.0023$) (Fig. 7 *D* and *E*). We next compared the modulation of dendritic plateau potentials by inhibition applied to on branch, and on the neighboring dendrite (off branch) (Fig. 7*F*). GABA uncaging at both locations reduced the peak amplitudes of the plateau potentials comparably (on branch: 88 ± 4%, $n = 10$; off branch: 95 ± 1%, $n = 7$, Mann–Whitney, $P = 0.4173$) (Fig. 7 *G* and *H*). As expected, on-branch stimulation was significantly more effective than off-branch stimulation in reducing the duration of the plateau potentials (Δ*duration*: on branch: 40 ± 3%, $n = 10$; off branch: 11 ± 3%, $n = 7$, Mann–Whitney, $P = 0.0008$) (Fig. 7 *H* and *I*). In addition, on-branch GABA uncaging elicited larger Δ*Vm* and Δ*area* compared with the same uncaging protocol applied to off-branch locations (Δ*Vm*: on branch: 4.7 ± 0.5 mV, $n = 10$; off branch: 1.9 ± 0.3 mV, $n = 7$, Mann–Whitney, $P = 0.0015$; Δ*area*: on branch: 552 ± 93 mV × ms, $n = 10$; off branch: 238 ± 63 mV × ms, $n = 7$, Mann–Whitney, $P = 0.033$) (Fig. 7 *I* and *J*). The Δ*Vm* obtained from experiments matched with our modeling predictions (Fig. 7*I* and *SI Appendix*, Fig. S9 *F* and *G*). Taken together, these data confirmed that the efficacy of GABA inhibition is dendritic location-specific.

Finally, we performed the same experiments in Mg^2-free conditions. In Mg^{2+}-free ACSF, there was no noticeable difference in the resting membrane potential and in the amplitude of uIPSCs, while the decay time constants of uEPSCs were prolonged due to removal

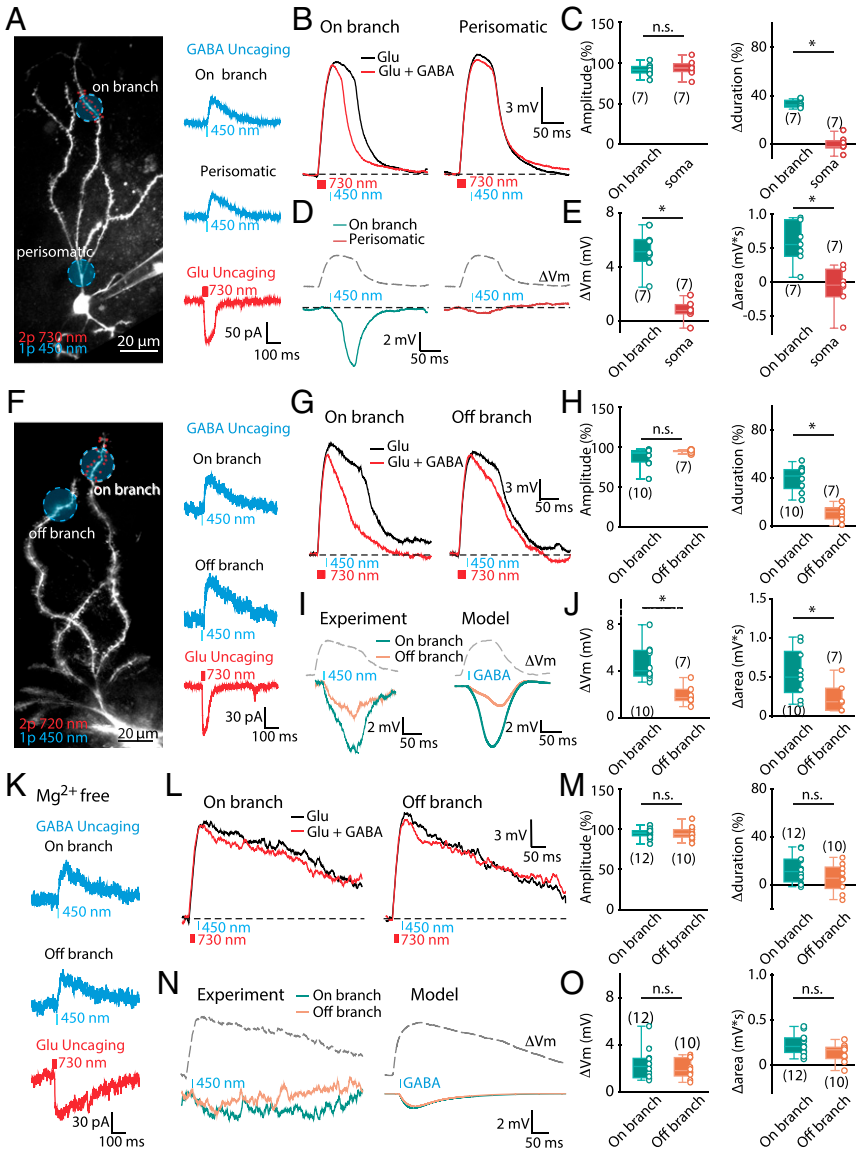

Fig. 7. Location-specific inhibition is dependent on the Mg^{2+} block of NMDAR. (*A*, *Left*) Experimental configuration illustrating locations for Glu-2PLU (red dots) and 1P GABA uncaging (blue area). (*Right*) uIPSCs (blue) and uEPSC (red) evoked by one-photon GABA and Glu-2PLU, respectively. (*B*) Representative traces of dendritic plateaus induced by Glu-2PLU caging (black) and subsequent one-photon GABA uncaging (red) at on-branch (*Left*) or perisomatic (*Right*) locations. (*C*) The effect of GABA uncaging on the peak amplitude ($P = 0.7104$) and Δ*duration* ($P = 0.0006$) of the dendritic plateau potentials. (*D*) Δ*Vm* was obtained via subtraction of plateau potentials with (red) and without (black) GABA uncaging in *B*. (*E*) Δ*Vm* and Δ*area* were significantly larger when the $GABA_AR$ was activated at on branch than perisomatic locations ($P = 0.006$ and 0.0023). (*F*, *Left*) Experimental configuration illustrating locations for 2 Glu-2PLU. (*Right*) Representative uIPSCs (blue) and uEPSC (red). (*G*) Representative traces of dendritic plateau potentials induced by Glu-2PLU (black) and subsequent one-photon GABA uncaging (red) at on-branch (*Left*) or off-branch (*Right*) locations. (*H*) The effect of GABA uncaging on the peak amplitude ($P = 0.4173$) and Δ*duration* ($P = 0.0008$) of the dendritic plateau potentials. (*I*) Experimental and modeled Δ*Vm* were obtained via subtraction of plateau potentials with and without GABA uncaging. (*J*) Δ*Vm* was significantly larger when the $GABA_AR$ was activated at on-branch than off-branch locations ($P = 0.0015$ and 0.033). (*K*) Representative traces of uIPSCs and uEPSC recorded in Mg^{2+}-free ACSF. (*L*) Representative traces of dendritic plateau potentials induced by Glu-2PLU with (black) and without (red) on- or off-branch one-photon GABA uncaging in Mg^{2+}-free ACSF. (*M*) The effect of GABA uncaging on the peak amplitude ($P = 0.7713$) and Δ*duration* ($P = 0.2766$) of the dendritic plateau potentials. (*N*) Experimental and modeled Δ*Vm* in Mg^{2+}-free conditions. (*O*) No significant difference in Δ*Vm* ($P = 0.7667$) and Δ*area* ($P = 0.1145$) between on- and off-branch GABA uncaging. Gray dashed line: rescaled plateau potential to indicate the timing. *$P <$ 0.05; n.s., no significant difference.

of the Mg^{2+} block of NMDARs (Fig. 7*K*). We could evoke a plateau potential with much longer duration (ACSF: 93 ± 7 ms, $n = 10$; Mg^{2+}-free: 257 ± 50 ms, $n = 12$; Mann–Whitney, $P = 0.0003$) (Fig. 7*L*) with fewer spines activated (10 spines). When GABA uncaging was applied to on- and off-branch locations, peak membrane potential was slightly reduced in both cases (on branch: 95 ± 2% of Glu alone, $n = 12$, Wilcoxon, $P = 0.016$; off branch: 95 ± 3% Glu alone, $n = 10$, Wilcoxon, $P = 0.105$; on vs. off: Mann–Whitney, $P = 0.7713$) (Fig. 7 *L* and *M*). However, the difference in Δ*duration* between on- and off-branch GABA uncaging was no longer observed (Δ*duration*: on branch: 12 ± 3%, $n = 12$; off branch: 6 ± 4%, $n = 10$, Mann–Whitney, $P = 0.2766$) (Fig. 7 *L* and *M*). Finally, we calculated the Δ*Vm* and Δ*area* produced by on- and off-branch GABA uncaging. The measured Δ*Vm* and Δ*area* confirmed our model predictions (Fig. 7*N* and *SI Appendix*, Fig. S9*H*). There was no significant difference in Δ*Vm* and Δ*area* between on- and off-branch GABA uncaging (Δ*Vm*: on branch: 2.4 ± 0.4 mV, $n = 12$; off branch: 2.0 ± 0.3, n =10, Mann–Whitney, $P = 0.7667$; Δ*area*: on branch: 233 ± 36 mV × ms, $n = 12$; perisomatic: 138 ± 31 mV × ms, $n = 10$, Mann–Whitney, $P = 0.1145$) (Fig. 7*O*). In summary, these experimental results confirmed our model predictions and indicated that dendritic branch-specific inhibition of a plateau potential is indeed enabled through the Mg^{2+} block of NMDARs.

Discussion

Dendritic plateau potentials are long-lasting depolarizations which can be evoked by spatially and temporally clustered excitatory inputs at distal dendrites in SPNs (8). In this study, we combined computational and experimental approaches to investigate how plateau potentials interact with subsequent excitatory and inhibitory inputs. We found that the plateau potential can broaden spatiotemporal integration of excitatory inputs and promote spiking (Fig. 2). The shapes of plateau potentials, as well as the spike outputs, are also fine-tuned by inhibition (Fig. 3). Such tunable spatiotemporal windows for inhibition can be achieved in a cell-type–specific manner, which was directly validated by combined 2PLU glutamate uncaging and optogenetic stimulation (Fig. 4). We next explored the principles and ionic mechanisms underlying the spatiotemporal windows with simulations and predicted that the Mg^{2+}-block of NMDARs accounts for the optimal window of inhibition. Finally by using dual-color two-photon glutamate and one-photon GABA uncaging, we directly demonstrated that a small hyperpolarization caused by local GABAergic input is critical for reestablishing NMDAR Mg^{2+}-block and hence dendritic compartmentalized and branch-specific inhibition on plateau potentials in the SPNs (Fig. 7).

Dendritic Nonlinearities in SPNs. Dendritic nonlinearity enables a single neuron to function as a multilayer computational device in which individual dendritic branches serve as the computational unit (1, 2, 49, 50). Many fundamental differences exist between pyramidal neuron types and SPNs. For example, the pyramidal neurons have apical dendrites on which a higher density of dendritic voltage-gated Na^+ channels is expressed. The dendritic Na^+ channel boosts the integration of inputs (1, 48) and favors action potential back-propagation (51). The SPN dendrites, however, do not have a basal/apical arrangement (8, 52) and express high amounts of Kir channels, making the resting membrane potential much more hyperpolarized and the dendritic membrane much leakier than in pyramidal neurons (14, 15). Moreover, the sodium spikelet, a hallmark of NMDA spikes/plateaus in pyramidal neurons (47, 53), appears to be absent in the dendritic plateau potential evoked in SPNs (8).

Despite SPNs receiving convergent excitatory inputs from various parts of the cerebral cortex and thalamus, each unitary excitatory input is small, typically 10–20 pA (54). To reach spike threshold, SPN membrane potentials have to go through a 20- to 30-mV subthreshold depolarization. If summed linearly, this would require the synchronized excitatory drive of a large number (hundreds or thousands) of inputs to evoke action potentials. Dendritic nonlinearities can efficiently drive SPNs to rapidly transition from the down-state to the up-state, allowing SPNs to integrate temporally delayed and spatially distant excitatory inputs and to transform subthreshold signals into spikes (Fig. 2). There are several advantages for this form of nonlinearity. First, it is highly efficient because the synchronous activation of only a few synapses (tens) is sufficient to induce a plateau potential and spiking (8). Second, it can strengthen the spatial integration of cortical inputs, regardless of the dendritic location (Fig. 2*E*), enabling neuron-wide integration for excitation. Third, the dendritic nonlinearity can broaden the temporal integration window, allowing delayed excitatory inputs to be efficiently integrated. Finally, compartmentalized dendritic plateau potentials in SPNs may facilitate long-term plasticity and be critical for motor learning and action selection.

Nonlinear Inhibition of Dendritic Plateau Potential. A unique feature of SPNs is that they are principal neurons in an almost entirely inhibitory microcircuit. SPNs receive inhibitory inputs from three major inhibitory sources: PV-positive FS interneurons, SST-/NPY-positive LTS interneurons, and neighboring SPNs (18, 19, 27). In this study, we revealed that these striatal inhibitory inputs could display distinct effects on synaptic excitation through dendritic nonlinearities.

FS interneuron-mediated perisomatic inhibition was generally believed to strongly inhibit SPN firing, enabling FS interneurons to powerfully innervate the striatal network (18, 19). However, our simulation showed that individual input from FS interneurons had little effect on plateau-coupled excitation. This finding suggests that the main role for FS interneurons is to regulate the somatic membrane potential rather than switching off plateau potentials (Fig. 3 *C* and *D*). Therefore, dendritic plateau potentials could be sustained despite FS-mediated inhibition. Another interesting finding is the very effective inhibition mediated by GABAergic IPSCs with slow kinetics, presumably mediated by NPY-NGF interneurons (26, 55). Dendritic slow GABAergic IPSCs showed the strongest efficacy in dendritic inhibition (Figs. 3 and 7). Although NPY-NGF interneurons are sparsely distributed in the striatum, considering the reported high-connectivity to SPNs (~60–87%) (26, 55), single NPY-NGF interneurons might possess more powerful inhibition to the striatal network than we expected.

Finally, the subtle control of dendritic nonlinearities of SPNs is from dendritic GABAergic input with fast kinetic: that is, collateral inhibition of neighboring SPNs and dendritic inhibition of SST-/NPY-positive LTS interneurons (27). Previous theoretical studies have predicted that dendritic inhibition in cortical pyramidal neurons could prevent initiation (31) or completely shut down the dendritic plateau potential (30). Here, we provided mechanistic insights on how inhibition interacts with dendritic nonlinearities. In addition to completely shutting down the plateau potentials, we found that local inhibition fine-tuned the plateau potential in a timing-dependent manner, suggesting collateral and LTS-mediated inhibition are involved in regulating dendritic nonlinearities of SPNs.

Inhibition also Involves NMDAR Mg^{2+}-Block. Our theoretical understanding of dendritic inhibition is largely grounded on Cable theory and shunting effects of GABA. For example, Koch et al. proposed the proximal (on-path) inhibition could yield the strongest effects on the excitation (43). In contrast, Gidon and Segev predicted that distal inhibition could better "shunt" a group of excitatory synapses (56). Here, we tested similar ideas in our simulations (*SI Appendix*, Fig. S3*A*) and found that all of these distribution of GABA channels are less effective in inhibiting the plateau potentials compared with activating few on-site GABA channels, in a particular temporal window (*SI Appendix*, Fig. S3 *C* and *D*).

Induction of plateau potentials generally requires clustered activation of 10–20 spines at a single branch in experimental conditions (8, 47). Due to slow decay kinetics (τ_{decay} = ~100 ms), fully opened NMDA channels generate a large synaptic conductance (~30–50 nS) in the branch, persistently bringing inward currents and depolarizing the dendrite (*SI Appendix*, Fig. S7*C*). In contrast, typical dendritically targeted inhibition (e.g., collateral inhibition) has small conductance (on the order of ~1 nS) and acts transiently (τ_{decay} = ~10 ms). In theory, one inhibitory synapse at the plateau site could only generate a small membrane potential perturbation in the branch. Thus, the shunting inhibition alone cannot counteract against the dendritic plateau potential (Fig. 7 *L* and *N*). However, such perturbation can immediately impact NMDARs and cause reestablishment of Mg^{2+} block and thus boost the inhibition effect (Fig. 6 *C* and *D*).

Taking these data together, our study suggests that the impact of dendritic inhibition might depend on the spatiotemporal structure of excitatory inputs. As NMDA spikes/plateau potentials are important for learning and memory (5–7), its controlling mechanism—cell-type–specific inhibition and NMDAR Mg^{2+}-block–dependent inhibition—is expected to play significant roles in shaping fine details of information integration.

Materials and Methods

Adult mice (5–9 wk, male and female) were used for this study. PV-Cre mice (Jackson Laboratory) and A2a-Cre mice (Mutant Mouse Research Resource Center) were used for viral injections. All procedures were approved by Stanford University's Administrative Panel on Laboratory Animal Care. Oblique horizontal brain slices (300 μm) containing the dorsal striatum were obtained from mice of both gender using standard techniques. Detailed information about modeling, imaging, and electrophysiology is included in *SI Appendix*.

ACKNOWLEDGMENTS. We thank members of the J.B.D. and J.H.K. laboratories for helpful discussions. This work was supported by National Institute of Neurological Disorders and Stroke/NIH Grant NS091144 (to J.B.D.); National Institute of Alcohol Abuse and Alcoholism/NIH Grant AA025721 (to J.B.D.); and the GG Technologies endowed research fund (J.B.D.). B.R. and G.K. have received grants from the European Union (Grants ERC-682426, FP7-323945, and H2020-712821); the Hungarian Research, Development and Innovation Office (Grants VKSZ_14-1-2015-0155, KFI_16-1-2016-0177, and NVKP_16-1-2016-0043); and the Hungarian Government (Grants KTIA_NAP_12-2-2015-0006, KMR_12-1-2012-0214, SH/7/2/8, and GINOP_2.1.1-15-2016-00979). Y.-W.W. is supported by a Parkinson's Disease Foundation postdoctoral fellowship (Grant PDF-FBS-1556). K.D., R.L., and J.H.K. have received grants from the European Horizon2020 Framework Programme [Grant 720270 (Human Brain Project SGA1)], the Swedish Research Council, the National Institute on Alcohol Abuse and Alcoholism (Grant 2R01AA016022), and the Swedish e-Science Research Center.

1. Major G, Larkum ME, Schiller J (2013) Active properties of neocortical pyramidal neuron dendrites. *Annu Rev Neurosci* 36:1–24.
2. Stuart GJ, Spruston N (2015) Dendritic integration: 60 years of progress. *Nat Neurosci* 18:1713–1721.
3. London M, Häusser M (2005) Dendritic computation. *Annu Rev Neurosci* 28:503–532.
4. Silver RA (2010) Neuronal arithmetic. *Nat Rev Neurosci* 11:474–489.
5. Xu NL, et al. (2012) Nonlinear dendritic integration of sensory and motor input during an active sensing task. *Nature* 492:247–251.
6. Gambino F, et al. (2014) Sensory-evoked LTP driven by dendritic plateau potentials in vivo. *Nature* 515:116–119.

7. Lavzin M, Rapoport S, Polsky A, Garion L, Schiller J (2012) Nonlinear dendritic processing determines angular tuning of barrel cortex neurons in vivo. *Nature* 490:397–401.
8. Plotkin JL, Day M, Surmeier DJ (2011) Synaptically driven state transitions in distal dendrites of striatal spiny neurons. *Nat Neurosci* 14:881–888.
9. Smith AD, Bolam JP (1990) The neural network of the basal ganglia as revealed by the study of synaptic connections of identified neurones. *Trends Neurosci* 13:259–265.
10. Gerfen CR (1992) The neostriatal mosaic: Multiple levels of compartmental organization in the basal ganglia. *Annu Rev Neurosci* 15:285–320.
11. Smith Y, Raju DV, Pare JF, Sidibe M (2004) The thalamostriatal system: A highly specific network of the basal ganglia circuitry. *Trends Neurosci* 27:520–527.
12. Graybiel AM (2005) The basal ganglia: Learning new tricks and loving it. *Curr Opin Neurobiol* 15:638–644.
13. Graybiel AM, Aosaki T, Flaherty AW, Kimura M (1994) The basal ganglia and adaptive motor control. *Science* 265:1826–1831.
14. Wilson CJ, Kawaguchi Y (1996) The origins of two-state spontaneous membrane potential fluctuations of neostriatal spiny neurons. *J Neurosci* 16:2397–2410.
15. Stern EA, Kincaid AE, Wilson CJ (1997) Spontaneous subthreshold membrane potential fluctuations and action potential variability of rat corticostriatal and striatal neurons in vivo. *J Neurophysiol* 77:1697–1715.
16. Stern EA, Jaeger D, Wilson CJ (1998) Membrane potential synchrony of simultaneously recorded striatal spiny neurons in vivo. *Nature* 394:475–478.
17. Wolf JA, et al. (2005) NMDA/AMPA ratio impacts state transitions and entrainment to oscillations in a computational model of the nucleus accumbens medium spiny projection neuron. *J Neurosci* 25:9080–9095.
18. Gittis AH, Kreitzer AC (2012) Striatal microcircuitry and movement disorders. *Trends Neurosci* 35:557–564.
19. Tepper JM, Koós T, Wilson CJ (2004) GABAergic microcircuits in the neostriatum. *Trends Neurosci* 27:662–669.
20. Koós T, Tepper JM (1999) Inhibitory control of neostriatal projection neurons by GABAergic interneurons. *Nat Neurosci* 2:467–472.
21. Kita H, Kosaka T, Heizmann CW (1990) Parvalbumin-immunoreactive neurons in the rat neostriatum: A light and electron microscopic study. *Brain Res* 536:1–15.
22. Koos T, Tepper JM, Wilson CJ (2004) Comparison of IPSCs evoked by spiny and fast-spiking neurons in the neostriatum. *J Neurosci* 24:7916–7922.
23. Kawaguchi Y (1993) Physiological, morphological, and histochemical characterization of three classes of interneurons in rat neostriatum. *J Neurosci* 13:4908–4923.
24. Gittis AH, Nelson AB, Thwin MT, Palop JJ, Kreitzer AC (2010) Distinct roles of GABAergic interneurons in the regulation of striatal output pathways. *J Neurosci* 30:2223–2234.
25. Kubota Y, Kawaguchi Y (2000) Dependence of GABAergic synaptic areas on the interneuron type and target size. *J Neurosci* 20:375–386.
26. Ibáñez-Sandoval O, et al. (2011) A novel functionally distinct subtype of striatal neuropeptide Y interneuron. *J Neurosci* 31:16757–16769.
27. Straub C, et al. (2016) Principles of synaptic organization of GABAergic interneurons in the striatum. *Neuron* 92:84–92.
28. Planert H, Szydlowski SN, Hjorth JJJ, Grillner S, Silberberg G (2010) Dynamics of synaptic transmission between fast-spiking interneurons and striatal projection neurons of the direct and indirect pathways. *J Neurosci* 30:3499–3507.
29. Czubayko U, Plenz D (2002) Fast synaptic transmission between striatal spiny projection neurons. *Proc Natl Acad Sci USA* 99:15764–15769.
30. Farinella M, Ruedt DT, Gleeson P, Lanore F, Silver RA (2014) Glutamate-bound NMDARs arising from in vivo-like network activity extend spatio-temporal integration in a L5 cortical pyramidal cell model. *PLOS Comput Biol* 10:e1003590.
31. Rhodes P (2006) The properties and implications of NMDA spikes in neocortical pyramidal cells. *J Neurosci* 26:6704–6715.
32. Kemp JM, Powell TP (1971) The termination of fibres from the cerebral cortex and thalamus upon dendritic spines in the caudate nucleus: A study with the Golgi method. *Philos Trans R Soc Lond B Biol Sci* 262:429–439.
33. Ascoli GA, Donohue DE, Halavi M (2007) NeuroMorpho.Org: A central resource for neuronal morphologies. *J Neurosci* 27:9247–9251.
34. Gerfen CR, Surmeier DJ (2011) Modulation of striatal projection systems by dopamine. *Annu Rev Neurosci* 34:441–466.
35. Evans RC, et al. (2012) The effects of NMDA subunit composition on calcium influx and spike timing-dependent plasticity in striatal medium spiny neurons. *PLOS Comput Biol* 8:e1002493.
36. Paille V, et al. (2013) GABAergic circuits control spike-timing-dependent plasticity. *J Neurosci* 33:9353–9363.
37. Wu YW, et al. (2015) Input- and cell-type-specific endocannabinoid-dependent LTD in the striatum. *Cell Reports* 10:75–87.
38. Matyas F, et al. (2010) Motor control by sensory cortex. *Science* 330:1240–1243.
39. Galarreta M, Hestrin S (1998) Frequency-dependent synaptic depression and the balance of excitation and inhibition in the neocortex. *Nat Neurosci* 1:587–594.
40. Taverna S, Ilijic E, Surmeier DJ (2008) Recurrent collateral connections of striatal medium spiny neurons are disrupted in models of Parkinson's disease. *J Neurosci* 28:5504–5512.
41. Mel BW, Schiller J (2004) On the fight between excitation and inhibition: Location is everything. *Sci STKE* 2004:PE44.
42. Liu G (2004) Local structural balance and functional interaction of excitatory and inhibitory synapses in hippocampal dendrites. *Nat Neurosci* 7:373–379.
43. Koch C, Poggio T, Torre V (1983) Nonlinear interactions in a dendritic tree: Localization, timing, and role in information processing. *Proc Natl Acad Sci USA* 80:2799–2802.
44. Fino E, et al. (2009) RuBi-glutamate: Two-photon and visible-light photoactivation of neurons and dendritic spines. *Front Neural Circuits* 3:2.
45. Chiovini B, et al. (2014) Dendritic spikes induce ripples in parvalbumin interneurons during hippocampal sharp waves. *Neuron* 82:908–924.
46. Rall W, Rinzel J (1973) Branch input resistance and steady attenuation for input to one branch of a dendritic neuron model. *Biophys J* 13:648–687.
47. Schiller J, Major G, Koester HJ, Schiller Y (2000) NMDA spikes in basal dendrites of cortical pyramidal neurons. *Nature* 404:285–289.
48. Larkum ME, Nevian T, Sandler M, Polsky A, Schiller J (2009) Synaptic integration in tuft dendrites of layer 5 pyramidal neurons: A new unifying principle. *Science* 325:756–760.
49. Lovett-Barron M, et al. (2012) Regulation of neuronal input transformations by tunable dendritic inhibition. *Nat Neurosci* 15:423–430, S421-423.
50. Poirazi P, Brannon T, Mel BW (2003) Arithmetic of subthreshold synaptic summation in a model CA1 pyramidal cell. *Neuron* 37:977–987.
51. Day M, et al. (2006) Selective elimination of glutamatergic synapses on striatopallidal neurons in Parkinson disease models. *Nat Neurosci* 9:251–259.
52. MacAskill AF, Little JP, Cassel JM, Carter AG (2012) Subcellular connectivity underlies pathway-specific signaling in the nucleus accumbens. *Nat Neurosci* 15:1624–1626.
53. Schiller J, Schiller Y (2001) NMDA receptor-mediated dendritic spikes and coincident signal amplification. *Curr Opin Neurobiol* 11:343–348.
54. Ding J, Peterson JD, Surmeier DJ (2008) Corticostriatal and thalamostriatal synapses have distinctive properties. *J Neurosci* 28:6483–6492.
55. Luo R, Janssen MJ, Partridge JG, Vicini S (2013) Direct and GABA-mediated indirect effects of nicotinic ACh receptor agonists on striatal neurones. *J Physiol* 591:203–217.
56. Gidon A, Segev I (2012) Principles governing the operation of synaptic inhibition in dendrites. *Neuron* 75:330–341.